Carcinogenesis vol.33 no.8 pp.1553–1562, 2012
doi:10.1093/carcin/bgs180
Advance Access Publication May 18, 2012

Release of TGFβig-h3 by gastric myofibroblasts slows tumor growth and is decreased with cancer progression

Chris Holmberg[1], Michael Quante[2], Islay Steele[1], Jothi Dinesh Kumar[1], Silviya Balabanova[1], Cedric Duval[1], Matyas Czepan[3], Zoltan Rakonczay Jr[3], Laszlo Tiszlavicz[4], Istvan Nemeth[4], Gyorgy Lazar[5], Zsolt Simonka[5], Rosalind Jenkins[6], Peter Hegyi[3], Timothy C.Wang[7], Graham J.Dockray[1] and Andrea Varro[1,8,*]

[1]Department of Cellular & Molecular Physiology, Institute of Translational Medicine, University of Liverpool, Liverpool, UK, [2]II. Medizinische Klinik, Klinikum rechts der Isar, Technische Universität München, München, Germany, [3]First Department of Medicine, [4]First Department of Pathology and [5]First Department of Surgery, University of Szeged, Szeged, Hungary, [6]Department of Molecular & Clinical Pharmacology, Institute of Translational Medicine, University of Liverpool, Liverpool, UK, [7]Department of Medicine, Columbia University, New York, NY, USA and [8]Department of Molecular & Clinical Cancer Medicine, Institute of Translational Medicine, University of Liverpool, Liverpool, UK

[*]To whom correspondence should be addressed. Tel: +44 (0) 151 794 5331; Fax: +44 (0) 151 794 5315;
Email: avarro@liv.ac.uk

Tumor progression has been linked to changes in the stromal environment. Myofibroblasts are stromal cells that are often increased in tumors but their contribution to cancer progression is not well understood. Here, we show that the secretomes of myofibroblasts derived from gastric cancers [cancer-associated myofibroblasts (CAMs)] differ in a functionally significant manner from those derived from adjacent tissue [adjacent tissue myofibroblasts (ATMs)]. CAMs showed increased rates of migration and proliferation compared with ATMs or normal tissue myofibroblasts (NTMs). Moreover, conditioned medium (CM) from CAMs significantly stimulated migration, invasion and proliferation of gastric cancer cells compared with CM from ATMs or NTMs. Proteomic analysis of myofibroblast secretomes revealed decreased abundance of the extracellular matrix (ECM) adaptor protein like transforming growth factor-β-induced gene-h3 (TGFβig-h3) in CAMs, which was correlated with lymph node involvement and shorter survival. TGFβig-h3 inhibited IGF-II-stimulated migration and proliferation of both cancer cells and myofibroblasts, and suppressed IGF-II activation of p42/44 MAPkinase; TGFβig-h3 knockdown increased IGF-II- and CM-stimulated migration. Furthermore, administration of TGFβig-h3 inhibited myofibroblast-stimulated growth of gastric cancer xenografts. We conclude that stromal cells exert inhibitory as well as stimulatory effects on tumor cells; TGFβig-h3 is a stromal inhibitory factor that is decreased with progression of gastric cancers.

Introduction

Stromal cells are well recognized to play influential roles in determining tumor progression (1–4). Cancer-associated fibroblasts (CAFs) are an important stromal cell type with distinct properties (5–7) and recent work indicates that differences in gene expression in the stromal compartment predict clinical outcome and response to therapy (8–10). Many different stromal cell factors may contribute to the tumor microenvironment (6,11–14), but the changes that occur in stromal cell function with cancer progression remain poorly understood.

Abbreviations: ATM, adjacent tissue myofibroblasts; CAF, cancer-associated fibroblasts; CAM, cancer-associated myofibroblasts; IGF-II, insulin-like growth factor-II; NTM, normal tissue myofibroblasts; TGFβig-h3, transforming growth factor-β-induced gene-h3.

Myofibroblasts, also sometimes called activated fibroblasts, are considered to be a subclass of CAFs. They are present in normal tissue in low density, increase with inflammation, infection or tissue damage (15) and are responsible for secretion of extracellular matrix (ECM) proteins, matrix metalloproteinases, protease inhibitors, growth factors, cytokines and chemokines as well as cyclo-oxygenase products. Epigenetic changes have been detected in cancer-associated myofibroblasts (CAMs) from gastric adenocarcinoma compared with myofibroblasts derived from adjacent tissue (ATMs) providing a basis for understanding how gastric CAMs might differ from other myofibroblasts (16).

Gastric cancer is the second most frequent cause of cancer-related mortality in males worldwide, and is frequently associated with *Helicobacter pylori* infection of the gastric corpus (17,18). The progression to cancer occurs over many decades and is characterized by preneoplastic changes including gastritis, atrophy, intestinal metaplasia and spasmolytic peptide-expressing metaplasia, and dysplasia (19,20). Infection is also associated with increases in gastric myofibroblasts that may reflect increased insulin-like growth factor (IGF) activity through matrix metalloproteinase-7 degradation of IGF-binding protein-5 (21–23), as well as recruitment of bone marrow-derived cells (24,25).

Recent studies suggest a role in cancer progression for the ECM adaptor protein transforming growth factor-β-induced gene-h3 (TGFβig-h3; also known as βig-h3, TGFBI, βIGH3, keratoepithelin and MP78/70). The latter is a 68 kDa protein with four fasciclin-like domains and an RGD domain in the C-terminal region; it binds ECM proteins including collagen, fibronectin and laminin (26,27). TGFβig-h3 suppresses the growth of Chinese hamster ovary cells in nude mice (28) and mice null for TGFβig-h3 develop spontaneous tumors in a variety of organs (29); loss of TGFβig-h3 in ovarian cancer is associated with resistance to taxanes (30). However, the role of TGFβig-h3 in cancer remains uncertain since expression has been associated with increased aggressiveness of liver and colon cancer cells (31,32). In this study, we have characterized a panel of CAMs from gastric cancers and compared their secretomes with those of myofibroblasts from adjacent tissue. We report here that decreased secretion of TGFβig-h3 in CAMs is associated with lymph node involvement and shorter survival, and we show that TGFβig-h3 suppresses cancer cell migration and inhibits growth in a model of stroma-stimulated cancer growth *in vivo*.

Materials and methods

Materials

Human recombinant TGFβig-h3 and IGF-II were obtained from R&D Systems (Abingdon, Oxon, UK); siRNA for TGFβig-h3, and control scrambled sequences were purchased from Ambion (Austin, TX). Antibodies for alpha-smooth muscle actin (α-SMA), vimentin and desmin were purchased from RDI (Flanders, NJ); antibody for pancytokeratin was used from Dako (Ely, Cambridgeshire, UK). Antibodies for TGFβig-h3, and GAPDH were obtained from R&D Systems and Biodesign (Saco, ME), respectively. Cleaved caspase-3 antibody was purchased from New England Biolabs (Hertfordshire, UK). Antibodies for Bax, Bim and Bcl-2 were purchased from Santa Cruz Biotechnology (Santa Cruz, CA), Abcam (Cambridge, UK) and Dako, respectively. Antibodies for total and phosphorylated p42/44 were obtained from Cell Signaling (Beverly, MA). All other chemicals were purchased from Sigma (Poole, Dorset, UK).

Generation of human primary myofibroblasts

Human primary myofibroblasts were derived from resected gastric cancers (CAM) and adjacent tissue (ATM) obtained from patients undergoing surgery for gastric cancer (Supplementary Table 1, available at *Carcinogenesis* Online (16,23)). Tumor and adjacent tissues were characterized using the TNM classification (Supplementary Methods, available at *Carcinogenesis* Online)

for gastric cancer (33). Normal myofibroblasts (NTM) were generated from deceased transplant donors with normal gastric morphology. Tumor and normal tissues were characterized using a scoring system for myofibroblast morphology, architecture and number (Supplementary Methods, available at *Carcinogenesis* Online). For histopathological assessments, myofibroblasts were defined as stellate/spindle-shaped cells with consistent α-SMA and vimentin co-expression. Smooth muscle fibers were excluded based on their characteristic morphology. This study was approved by the Ethics Committee of the University of Szeged, Hungary. Myofibroblasts were cultured as described previously (23) and were used between passages 3 and 10. Conditioned medium (CM) was prepared from 1×10^6 myofibroblasts plated in 10 cm diameter dishes to give 80–90% confluency and collected after 24 h in 10 ml serum-free media.

Human gastric carcinoma cell lines

AGS cells (ATCC, Manassas, VA) and MKN45 gastric carcinoma cells (RIKEN, Ibaraki, Japan) were cultured as described previously (34).

Immunohistochemistry

Formalin-fixed, paraffin-embedded, tissue sections were processed for detection of α-SMA, vimentin and desmin after antigen recovery using Multivision Polymer Detection System (Thermo Scientific). For immunocytochemistry, cells were cultured in chamber slides, stained with α-SMA, vimentin, desmin and pancytokeratin followed by incubation with the appropriate fluorescein or Texas Red-labeled secondary antibodies raised in donkey (Jackson Immunoresearch, Soham, UK), and mounted with Vectashield containing 4′,6-diamidino-2-phenylindole (Vector Laboratories, Peterborough, UK). For visualization of F-actin, the primary antibody was substituted with 50 µg/ml tetramethyl rhodamine iso-thiocyanate-conjugated phalloidin. Slides were viewed using a Zeiss Axioplan-2 microscope (Zeiss Vision, Welwyn Garden City, UK). Images were captured using a JVC-3 charge-coupled device camera at ×40 magnification with KS300 software (Imaging Associates, Bicester, Oxfordshire, UK).

Migration, invasion, proliferation and apoptosis assays

Migration and invasion of primary human gastric myofibroblasts or cancer cells were studied in 8 µm pore chambers (BD Control Cell Culture Inserts or BD BioCoat Matrigel Invasion Chambers, respectively; BD Biosciences, Oxford, UK) as described previously (23,35). Incorporation of [^{3}H]-thymidine by human gastric myofibroblasts or AGS cells was studied using methods described previously (34). Additionally, proliferation was assessed by incorporation of BrdU (3 ng/ml) as described previously (23), or EdU (10 µM) according to the manufacturer's instruction (Invitrogen, Paisley, UK). Apoptosis was studied using cleaved caspase-3 antibody (New England Biolabs (Hertfordshire, UK).

Isobaric tagging for relative and absolute quantitation

Myofibroblast CM was concentrated to 500 µl, acetone precipitated and resuspended in 0.5 M triethylammonium bicarbonate (TEAB) in 0.1% sodium dodecyl sulfate. Myofibroblasts were lysed directly in TEAB/sodium dodecyl sulfate. Samples (100 µg) were labeled using the 4-plex iTRAQ® kit (AB SCIEX, Foster City, CA) according to manufacturer's instructions. Labeled samples were pre-fractionated using a PolyLC PolySULFOETHYL A (4.6 × 200 mm i.d.) cation exchange column using an Agilent 1100 HPLC system (Agilent Technologies, Santa Clara, CA). Samples were then analyzed using an LC Packings Ultimate nano-LC system run in-line with a QStar Pulsar i mass spectrometer (AB Sciex). Protein identification and quantification were performed using the ProteinPilot™ v3.0.1 software (AB Sciex). The Paragon algorithm was selected as the default search program, with the digestion agent set as trypsin and cysteine modification as methyl methanethiosulfonate. Proteins were reported based on the assignment of at least two tryptic peptides with a confidence >95%, or on the assignment of one tryptic peptide with a confidence >99% and a local false discovery rate calculated using the PSPEP algorithm of <1%. Proteins exhibiting a differential abundance in CAMs versus ATMs were calculated only on the assignment of at least two tryptic peptides using a Pro Group™ algorithm of ProteinPilot™. When comparing groups of patients, proteins that were identified in >80% in one of the groups were used in the analysis. Pathway analysis was performed using MetaCore® (GeneGo, St Joseph, MI).

Western blotting

Myofibroblast cell extracts were prepared in RIPA buffer containing protease and phosphatase inhibitors and proteins resolved by sodium dodecyl sulfate–polyacrylamide gel electrophoresis and processed for western blotting as described previously (22).

Knockdown of TGFβig-h3

Knockdown of TGFβig-h3 was performed using 35 µM of TGFβig-h3 siRNA, and negative control scrambled RNA, for 72 h by nucleofection using the NHDF transfection kit (Amaxa; Köln, Germany). The efficiency of the knockdown was verified by western blotting.

Xenograft studies in SCID mice

To study the effect of TGFβig-h3 on xenograft growth, 6- to 8-week-old immunocompromised mice (SCID, Jackson Laboratories, Bar Harbor, ME) were used for subcutaneous injection of tumor cells with or without CAMs. Gastric cancer cells (MKN45, 5×10^5) were injected alone, alone on the left flank and together with 2×10^5 myofibroblasts on the right flank (groups 1 and 2, respectively), or with TGFβig-h3 (1 µg per mouse per day) from day 0 by Alzet pump (groups 3 and 4, respectively). In a subset of the co-injected group, tumors were allowed to grow for 2 weeks before treatment with TGFβig-h3. Tumor size was monitored every 3 days for 4 weeks. Tumors were dissected, measured, fixed in 10% formalin or 4% paraformaldehyde (PFA), embedded in paraffin or OTC for frozen sections, and processed for hematoxylin/eosin staining or localization of α-SMA, using ABC avidin–biotin–DAB detection kit (Vector Labs) according to the supplied protocol.

Statistics

Results are expressed as mean ± standard error of the mean, unless otherwise stated. Student's *t*-test or analysis of variance (ANOVA; Systat Software Inc., Hounslow, London, UK) as appropriate was used to determine statistical significance of results and considered significant at $P < 0.05$, unless otherwise stated (see above for the statistical analysis of the proteomic data).

Results

Increased migration and proliferation of gastric cancer-derived myofibroblasts

The primary gastric tumors employed in this study exhibited increased numbers of myofibroblasts typically with disordered architecture and morphology compared with adjacent tissue or normal tissue (Supplementary Figure 1, available at *Carcinogenesis* Online). Tissues adjacent to the tumor resection margin exhibited a range of morphologies including chronic gastritis (7), intestinal metaplasia (2) and intestinal metaplasia with atrophy (3) (Supplementary Table 1, available at *Carcinogenesis* Online).

Cultured myofibroblasts derived from normal tissue, cancer or tissue adjacent to gastric tumors all expressed α-SMA and vimentin but not desmin, and they were negative for pancytokeratin (Figure 1A). Basal rates of CAM migration in Boyden chambers were consistently greater than those of NTMs or their ATM counterparts (Figure 1B). Moreover, compared with their respective ATMs, CAMs also exhibited increased BrdU incorporation (Figure 1C), which was attributable to shorter G_1 phase of the cell cycle (Figure 1D). There was no difference in rates of apoptosis determined by cleaved caspase-3 staining (Figure 1C and E).

Stimulation of cancer cell proliferation and migration by cancer-derived myofibroblasts

Interestingly, CM from both CAMs and ATMs, but not NTMs, resulted in epithelial–mesenchymal transition of gastric cancer AGS cells characterized by increased cell scattering (Figure 2A) and α-SMA expression (Figure 2B). Moreover, there was increased AGS cell migration (Figure 2C) and proliferation (Figure 2D) in response to CAM-CM and ATM-CM. The migration, invasion and proliferation responses to CAM-CM were consistently greater than those to their ATM counterparts. When CAMs were divided into groups based on tumor depth (pT1-2 versus pT3-4) there was no difference in the effect of CM on AGS cell proliferation (not shown). However, when CAMs were separated into groups based on lymph node involvement (pN0-1 versus pN2-4) the stimulation of [^{3}H]-thymidine incorporation was greater in response to CM from CAMs of patients with high lymph node involvement (Figure 2E).

Myofibroblast proteomes change during cancer progression

To identify proteins that might account for the different properties of CAMs compared with ATMs, we first examined the cellular proteomes of 11 pairs of cells using isobaric tagging for relative and absolute quantitation (iTRAQ) labeling followed by liquid chromatography–mass spectrometry/mass spectrometry (LC-MS/MS) identification of labeled tryptic peptides (Supplementary Table 2, available at *Carcinogenesis* Online). A total of 768 proteins were identified in at least 3 pairs of samples and a core set of 241 proteins were identified in all 11 pairs which included proteins

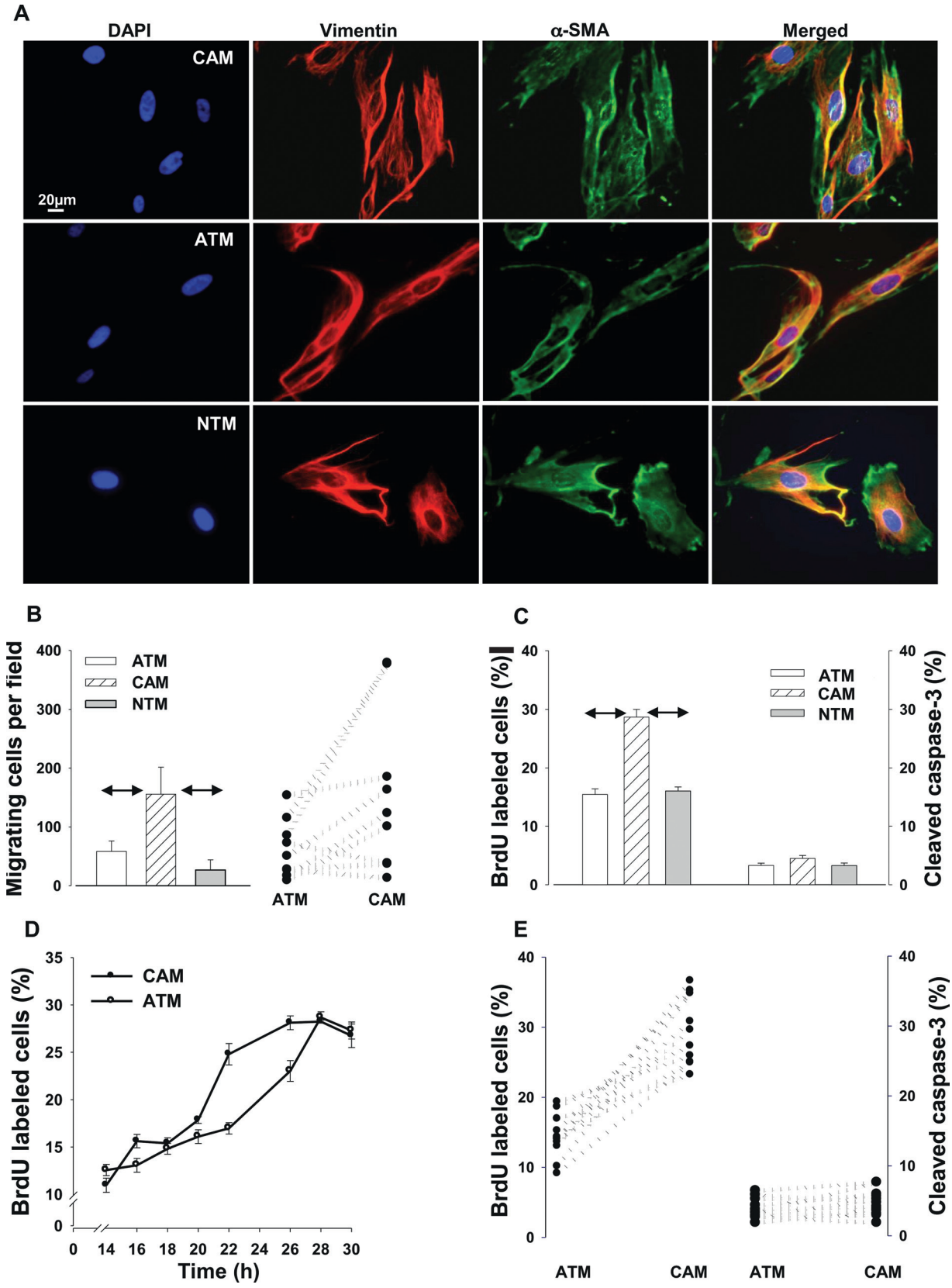

Fig. 1. Increased migration and proliferation of cultured gastric cancer-associated myofibroblasts. (**A**) Positive α-SMA (green) and vimentin (red) staining in cultured myofibroblasts (nuclear staining with 4′,6-diamidino-2-phenylindole, blue); top, CAMs; middle, ATMs; bottom, NTMs. (**B**) Increased migration of CAMs compared with ATMs and NTMs (left) in Boyden chambers, and individual pair-wise comparisons of CAMs versus their corresponding ATMs (right). (**C**) Increased BrdU labeling (left), but not apoptosis indicated by cleaved caspase-3 staining (right), in CAMs compared with ATMs and NTMs. (**D**) Shorter G_1 phase in CAMs compared with ATMs. (**E**) Individual pair-wise comparison of BrdU labeling and cleaved caspase-3 staining in CAMs versus their corresponding ATMs. Horizontal arrows, $P < 0.05$, ANOVA and $n = 10–14$.

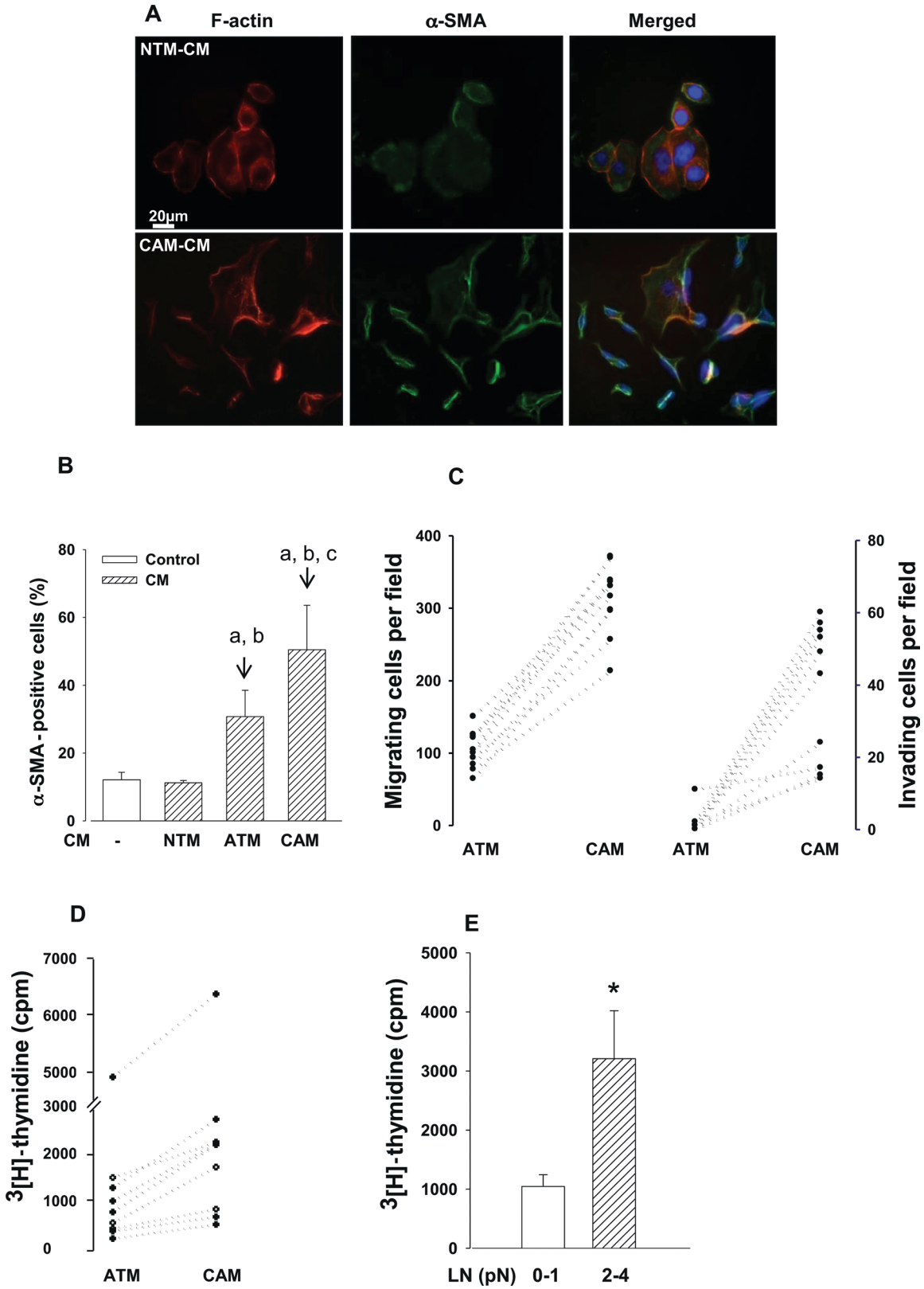

Fig. 2. Increased epithelial–mesenchymal transition, migration, invasion and proliferation of AGS cancer cells treated with CM from CAMs compared with ATMs. (**A**) Example of epithelial–mesenchymal transition characterized by scattering, α-SMA (green) and phalloidin staining (f-actin, red; nuclear staining with 4′,6-diamidino-2-phenylindole, blue) in AGS cells treated with CM from NTMs (top) compared with CAMs (bottom). (**B**) Quantification of α-SMA-positive AGS cells treated with CM from CAMs compared with ATMs and NTMs; a: $P < 0.05$ versus control, b: $P < 0.05$ versus NTM, c: $P < 0.05$ versus ATM (ANOVA). (**C**) Comparison of AGS cell migration (left) and invasion (right) in response to CM from paired samples of CAMs and ATMs. (**D**) ^{3}[H]-thymidine incorporation in AGS cells treated with CM from CAMs compared with their matched ATMs. (**E**) ^{3}[H]-thymidine incorporation in CAMs from patients with high (pN2-4) versus low or no (pN0-1) lymph node involvement; see Supplementary Methods, available at *Carcinogenesis* Online for details of the TNM classification. Horizontal arrows, ANOVA or *t*-test, $^{*}P < 0.05$ and $n = 10–14$.

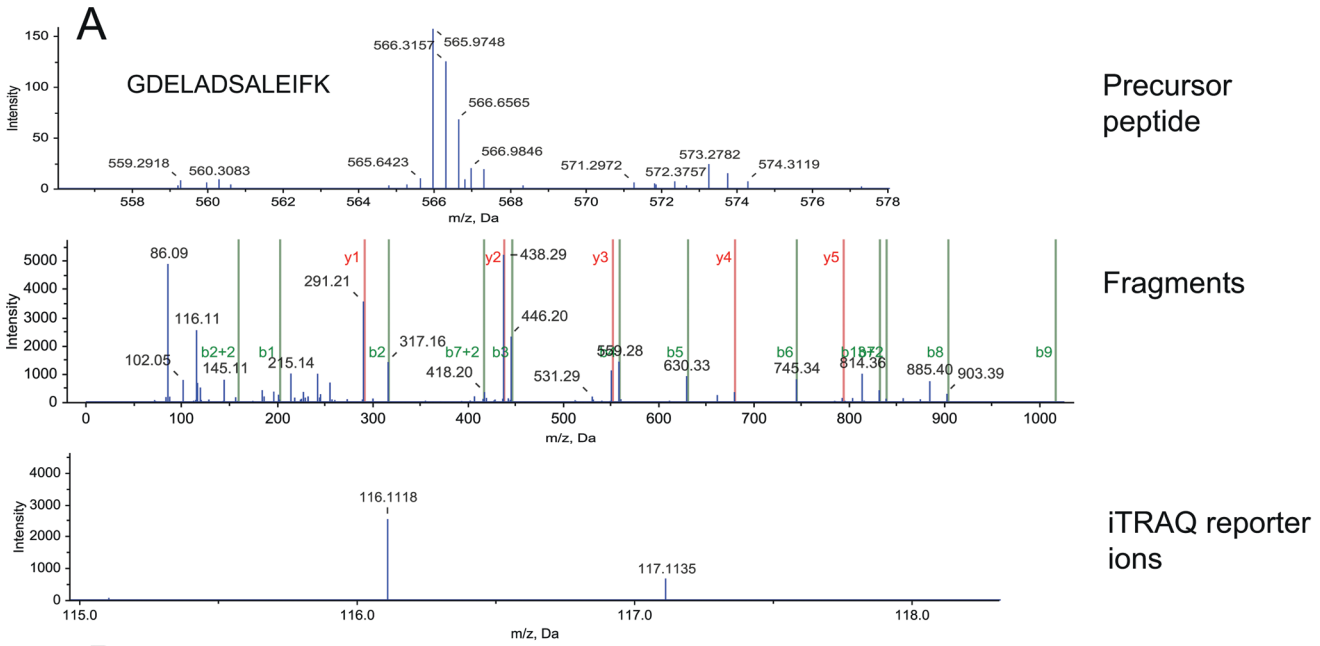

B

MALFVRLLAL ALALALGPAA TLAGPAKSPY QLVLQHSRLR GRQHGPNVCA VQKVIGTNRK YFTNCKQWYQ RKICGKSTVI
SYECCPGYEK VPGEKGCPAA LPLSNLYETL GVVGSTTTQL YTDRTEKLRP EMEGPGSFTI FAPSNEAWAS LPAEVLDSLV
SNVNIELLNA LRYHMVGRRV LTDELKHGMT LTSMYQNSNI QIHHYPNGIV TVNCARLLKA DHHATNGVVH LIDKVISTIT
NNIQQIIEIE DTFETLRAAV AASGLNTMLE GNGQYTLLAP TNEAFEKIPS ETLNRILGDP EALRDLLNNH ILKSAMCAEA
IVAGLSVETL EGTTLEVGCS GDMLTINGKA IISNKDILAT NGVIHYIDEL LIPDSAKTLF ELAAESDVST AIDLFRQAGL
GNHLSGSERL TLLAPLNSVF KDGTPPIDAH TRNLLRNHII KDQLASKYLY HGQTLETLGG KKLRVFVYRN SLCIENSCIA
AHDKRGRYGT LFTMDRVLTP PMGTVMDVLK GDNRFSMLVA AIQSAGLTET LNREGVYTVF APTNEAFRAL PPRERSRLLG
DAKELANILK YHIGDEILVS GGIGALVRLK SLQGDKLEVS LKNNVVSVNK EPVAEPDIMA TNGVVHVITN VLQPPANRPQ
ERGDELADSA LEIFKQASAF SRASQRSVRL APVYQKLLER MKH

C

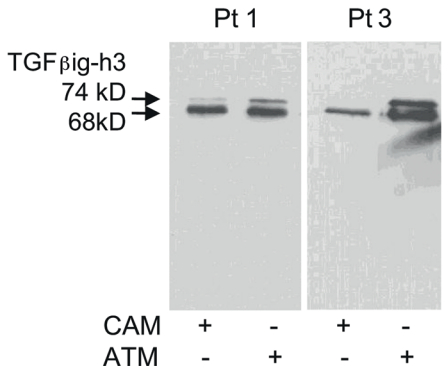

Fig. 3. Identification of TGFβig-h3 as differentially expressed in CAMs. (**A**) Representative spectra showing, top, identification of one of the precursor peptides for a typical tryptic fragment (GDELADSALEIFK); middle, identification of fragments of the precursor peptide; bottom, isobaric tagging for relative and absolute quantitation reporter ions for this identification. (**B**) The sequence of TGFβig-h3 showing in red the coverage of tryptic peptides identified in a representative sample; functional domains of the protein are underlined. (**C**) Representative western blots of TGFβig-h3 in media of CAMs and ATMs from patients with high (pN2-4) (right side) versus low or no (pN0-1) (left side) lymph node involvement showing depressed abundance in CAMs from the former.

that are putative myofibroblast markers including vimentin, cofilin and fibroblast activation protein-alpha (Supplementary Figure 2, available at *Carcinogenesis* Online) (36,37). Proteins exhibiting a significant difference in relative abundance were then analyzed by Metacore® (GeneGo) to identify *Process Networks* of differentially regulated interactions. Of 168 possible *Process Networks*, 39 were identified as significantly influenced. However, only one of these was significant in all 11 pairs of CAMs and ATMs (Supplementary Figure 3 and Supplementary Table 3, available at *Carcinogenesis* Online), namely the involvement of actin filaments, which is consistent with the observed differences between CAMs and ATMs in cell migration assays.

The contribution of myofibroblast secretomes to the tumor microenvironment

In order to identify directly the secreted proteins that might account for the properties of CAM CM, we then applied iTRAQ labeling followed by LC-MS/MS to myofibroblast media. Taking the secretomes of 11 pairs of CAMs and ATMs together, we identified 167 proteins that were expressed in three or more pairs of cells. Of these, 76 were considered secreted proteins using UniProt as the main database of which the largest categories were ECM proteins, proteases, binding proteins and ligands (Supplementary Figure 4, available at *Carcinogenesis* Online). Proteins exhibiting a differential abundance in CAMs versus ATMs varied between 12 and 42% of the total (Supplementary Table 4, available at *Carcinogenesis* Online). Interestingly, many of the differentially abundant proteins were decreased in CAMs, and included protease inhibitors and ECM-related proteins (Supplementary Table 4, available at *Carcinogenesis* Online). We then used Metacore® (with an MKN45 cell transcriptome as background) to identify candidate responses in cancer cells as a consequence of the differences in myofibroblast secretomes. Significant differences were found in 17 of 168 possible networks, of which 3 were significant in all 11 pairs of CAMs and ATMs (Supplementary Figure 5, available at *Carcinogenesis* Online). Importantly, given the biological properties of CM from CAMs in stimulating cancer cell invasion and migration, the three networks were associated with cell–matrix interactions, ECM remodeling and ECM degradation.

Secreted TGFβig-h3 from myofibroblast is linked to lymph node involvement and survival

We next analyzed the secretome data to identify candidate proteins exhibiting differences in abundance in CAMs from patients divided on the basis of low or no lymph node involvement (pN0-1) versus high lymph node involvement (pN2-4). The patients with high lymph node involvement had significantly shorter survival (9.6 ± 3.1 months) compared with patients with low or no lymph node involvement (44.0 ± 5.5 months, $P < 0.05$). Strikingly, in the dataset as a whole only a single protein, TGFβig-h3, exhibited a robust difference between the two groups (Fisher exact test with false discovery rate correction for multiple comparisons). Furthermore, TGFβig-h3 was one of the nodes in the cell–matrix interactions network, and also had interactions with nodes from the ECM remodeling and ECM degradation networks; thus, changes in TGFβig-h3 potentially influence all three of these signaling networks. The demonstration of TGFβig-h3 as decreased in CAMs from patients with high lymph node involvement was made on the basis of identification in all media samples with similar coverage in CAM and ATM samples (Figure 3B; Supplementary Table 5, available at *Carcinogenesis* Online). The finding was confirmed by western blot of media which revealed bands of approximately 68 and 72 kDa with decreased abundance in CAM media from patients with high lymph node involvement (Figure 3C).

TGFβig-h3 inhibits myofibroblast and cancer cell migration

To examine the consequence of TGFβig-h3 secretion by myofibroblasts, we then studied effects on cell migration and proliferation. Thus, TGFβig-h3 produced a concentration-dependent inhibition of IGF-II-stimulated migration of both myofibroblasts and AGS cells in Boyden chambers (Figure 4A). Similarly, IGF-II-stimulated myofibroblast and cancer cell proliferation was inhibited by TGFβig-h3 (1 μg/ml; Figure 4B). There was also increased cleaved caspase-3 in both myofibroblasts and cancer cells in response to TGFβig-h3 (Figure 4C); in the former, we showed associated increases in Bax and Bim, and decreased Bcl2, by western blot (Figure 4D).

To test whether TGFβig-h3 in myofibroblast media restrained IGF-II-stimulated migration, we examined the effects of siRNA knockdown. Treatment of myofibroblasts with TGFβig-h3 siRNA reduced the abundance of TGFβig-h3 detected by western blot of cell extracts by 64%, but did not change the abundance of another ECM protein, decorin, used as a negative control (Supplementary Figure 6, available at *Carcinogenesis* Online). In siRNA-treated cells, the stimulation of migration by IGF-II was enhanced indicative of an autocrine stimulatory role for IG-II (Figure 5A). To determine whether TGFβig-h3 released from myofibroblasts influenced cancer cell migration, we then examined CM from ATMs after prior treatment with TGFβig-h3 siRNA or control oligonucleotides. The stimulatory effect of myofibroblast CM on AGS cell migration was increased after TGFβig-h3 knockdown (Figure 5B), indicating that release of TGFβig-h3 inhibits growth factor-stimulated migration of both cancer cells and myofibroblasts. To elucidate the signaling pathways involved, we looked at the involvement of kinases downstream of the IGF-I receptor. Inhibition of p42/44 (U0126) activation significantly reduced IGF-II-stimulated myofibroblast migration and there was a smaller inhibition by a p38 kinase inhibitor (SB202190; Figure 5C), whereas the PI3-kinase (LY294002) and Jun-kinase (JNK-II) inhibitors had no or little effect; similar results were obtained in AGS cells (Supplementary Figure 7, available at *Carcinogenesis* Online). TGFβig-h3 inhibited IGF-II-stimulated phosphorylation of p42/44 kinase (Figure 5D).

TGFβig-h3 inhibits tumor growth in vivo

Finally, we asked whether TGFβig-h3 inhibited tumor growth *in vivo* using a xenograft model. For these studies, we used MKN45 cells that reproducibly establish tumors in a xenograft model and selected a CAM line (patient 3) that in preliminary studies stimulated MKN45 cell growth when coinjected in xenografts. Tumor growth after 4 weeks of MKN45 cells co-injected with CAMs (right side) was completely inhibited when TGFβig-h3 was administered for the duration of the experiment (Figure 6A and B). Moreover, there was even a reduction of approximately 85% of increased tumor mass when TGFβig-h3 was administered 2 weeks after the start of the experiment. There was no effect of TGFβig-h3 on tumor growth when MKN45 cells were injected in the absence of myofibroblasts, indicating that TGFβig-h3 prevents stromal cell-stimulated tumor growth even in established tumors. Interestingly, the TGFβig-h3-treated tumors exhibited more necrosis and less α-SMA-positive cells than their untreated counterparts (Figure 6A).

Discussion

Stromal cells drive tumor growth by multiple mechanisms influencing angiogenesis, inflammation and immune responses, as well as direct effects on tumor cells (12,14,37). We show here that gastric CAMs, which are a subset of CAFs, stimulate migration, proliferation and invasion of tumor cells compared with ATMs or NTMs; there are differences in the cellular proteomes and secretomes of CAMs and ATMs and we identify decreased secretion of the ECM protein TGFβig-h3 in CAMs from patients with high lymph node involvement and shorter survival. Cell migration and proliferation in response to IGF stimulation are inhibited by TGFβig-h3. Moreover, in a xenograft model, administration of TGFβig-h3 slows stroma-stimulated tumor growth. Thus, stromal cell secretion of an ECM protein provides a mechanism to inhibit tumor growth which is lost with tumor progression, indicating that stromal cells exhibit protective as well as aggressive properties.

There are differences in number, architecture and morphology of gastric CAMs compared with ATMs and NTMs; there are also functional differences when these cells are cultured. In principle, it is possible that cultured myofibroblasts might be unstable, but at least up to 10 passages we have found both the functional properties and molecular profiles of these cells to be stable. It becomes possible, then, to perform both functional studies and molecular profiling of secreted proteins in the same cells and to relate the findings to clinical data on cancer status. Although studies of stromal cell transcriptomes and proteomes can be carried out on microdissected tumor tissue, this approach does not lend itself to either concomitant functional studies in the same cells or kinetic analysis of the secreted proteins which determine the tumor microenvironment. These data indicate that in both cellular proteomes and in secretomes, there are differences between gastric CAMs and their corresponding ATMs consistent with observed functional differences, notably increased migration and inva-

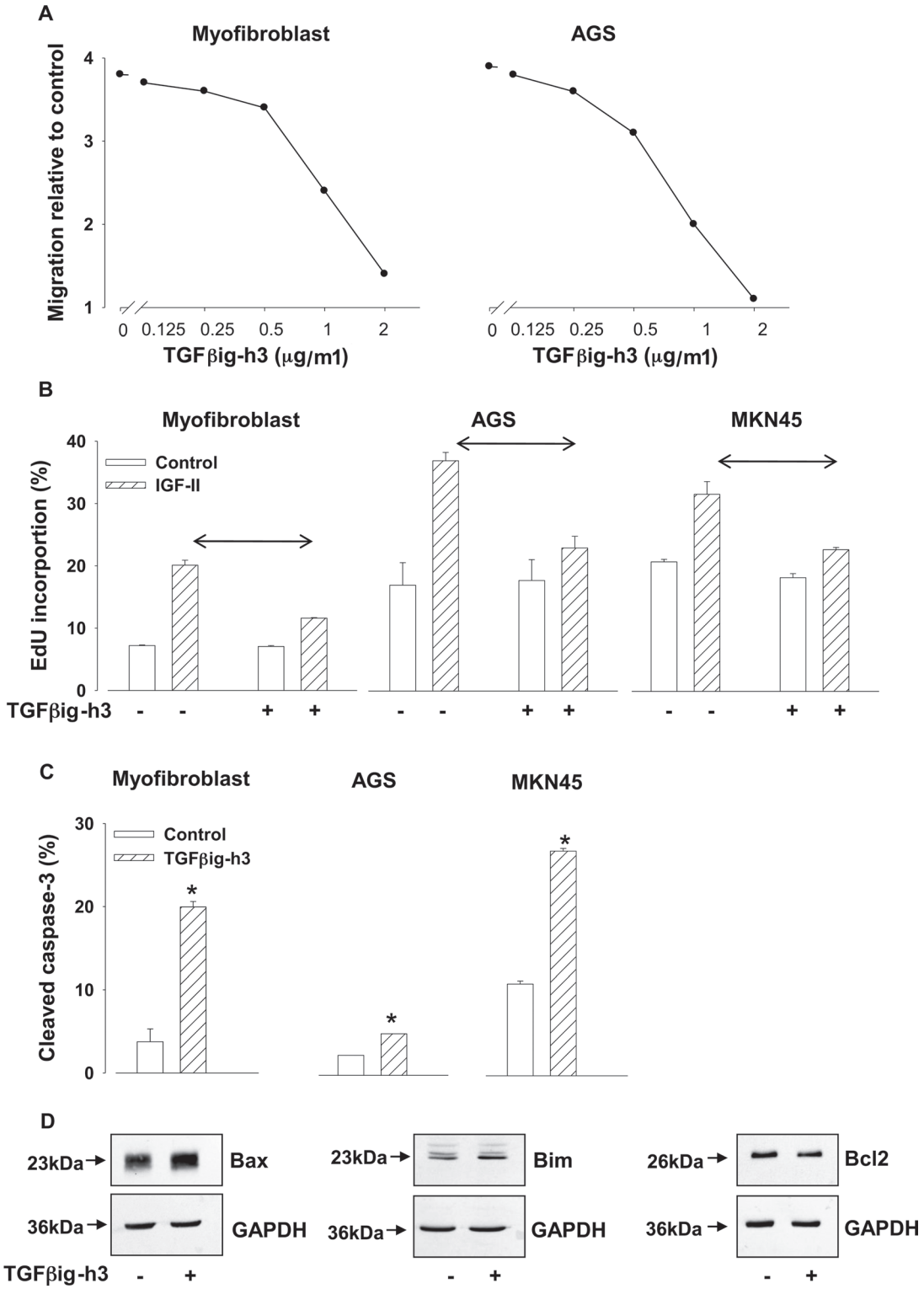

Fig. 4. Inhibition of myofibroblast and cancer cell proliferation and migration by TGFβig-h3 and stimulation of apoptosis. (**A**) Concentration-dependent inhibition of IGF-II (100 ng/ml)-stimulated myofibroblast and AGS cell migration by TGFβig-h3. (**B**) TGFβig-h3 (1 μg/ml) inhibition of IGF-II-stimulated myofibroblast, AGS and MKN45 cell proliferation determined by EdU incorporation. (**C**) TGFβig-h3 increased caspase-3 staining of myofibroblast, AGS and MKN45 cells. (**D**) TGFβig-h3 increased Bax and Bim in myofibroblasts detected by western blot and decreased Bcl-2. Horizontal arrows, ANOVA or *t*-test, $^*P < 0.05$ and $n = 3$.

sion by CAMs and by CAM CM applied to tumor cells. Moreover, a comparison of myofibroblast secretomes in patients with high versus low or no lymph node involvement revealed decreases in the ECM adaptor protein TGFβig-h3 in CAMs from advanced gastric tumors. The mechanism underlying loss of TGFβig-h3 remains uncertain, although examination of a microarray dataset indicates that mRNA abundance is unchanged (data not shown). This study was not designed to address differences in myofibroblast biology with respect to either tumor type (e.g. intestinal versus diffuse), or in preneoplastic changes (e.g. chronic gastritis, intestinal metaplasia and atrophy); nevertheless,

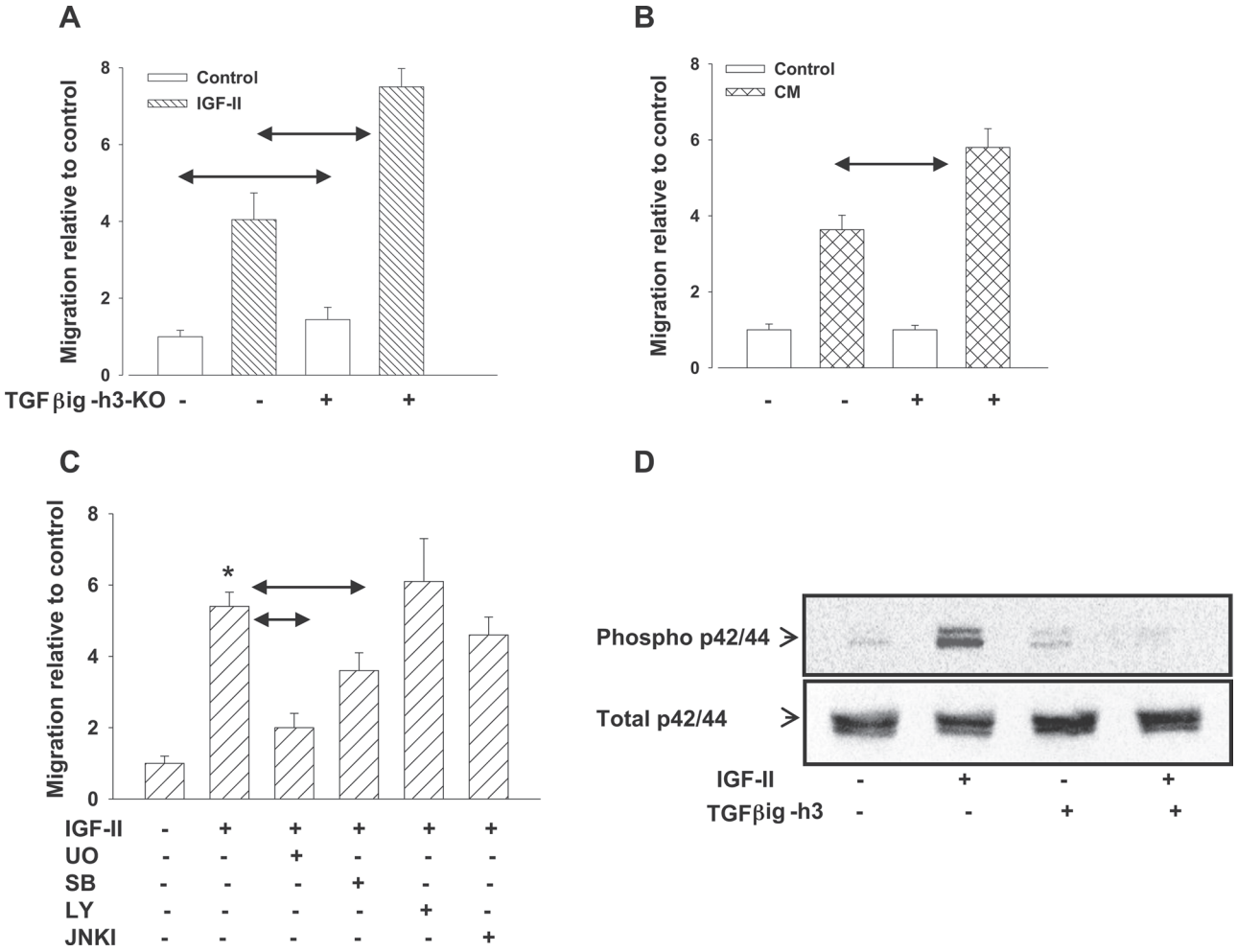

Fig. 5. Enhanced migration of myofibroblasts and AGS cells after knockdown of TGFβig-h3. (**A**) TGFβig-h3 siRNA knockdown (TGFβig-h3-KO) increased IGF-II (100 ng/ml)-stimulated myofibroblast migration. (**B**) CM from TGFβig-h3 siRNA-treated myofibroblasts increased AGS cell migration compared with CM from cells treated with control oligonucleotides. (**C**) IGF-II-stimulated myofibroblast migration is inhibited by U0126 (UO, 10 μM) and SB202190 (SB, 3 μM) but not LY294002 (LY, 50 μM) and JNK-II (JNK, 50 μM). (**D**) Representative western blot showing phosphorylation of p42/44 kinase was inhibited by TGFβig-h3. Horizontal arrows, $^*P < 0.05$ and $n = 3$.

our findings suggest that it is now both feasible and worthwhile to address these issues.

Myofibroblasts are well known to contribute to the deposition of ECM (38,39). These studies of myofibroblast secretomes indicate, however, that while some ECM proteins are increased in CAMs, others are decreased. Moreover, these differences are exaggerated in CAMs from patients with high lymph node involvement and poor survival, suggesting changes in CAM function as the disease progresses. In particular, there is an overall loss of diversity in the secretome with cancer progression and analysis of interaction networks indicates that these predict changes in cell behavior corresponding to functional changes observed *in vivo* notably with respect to cell migration and invasion.

It is only quite recently that proteomic approaches have been applied to the analysis of stromal cell secretomes (40). The identification of TGFβig-h3 as significantly decreased in the secretome of CAMs from patients with high lymph node involvement and short survival suggests a new dimension to the role of this protein in cancer. TGFβig-h3 was originally identified as a TGFβ-induced gene in the lung adenocarcinoma cell line A549 (26). There is accumulation of TGFβig-h3 at sites of inflammation and wound healing and it is thought to play a role in adhesion as a ligand of several integrins and by binding to collagen and other ECM proteins (27). Mutations of TGFβig-h3 are associated with corneal dystrophies (41,42), but its role in cancer is still unclear. Over-expression of TGFβig-h3 in Chinese hamster ovary cells decreased their tumor-forming capacity in nude mice (28), and a tumor suppressor function is indicated by the observation that mice null for TGFβig-h3 exhibit spontaneous tumors in a number of organs (29). Similarly, expression of TGFβig-h3 in ovarian cancer cells and in non-small cell lung cancer cells is associated with sensitivity to chemotherapy (30,43), and expression in neuroblastoma (44), lung and breast cancer cells (45,46) has been associated with decreased tumorigenicity. Conversely, however, TGFβig-h3 has been reported to promote invasion of colon and ovarian cancer cells (31,32,47). These studies have focused on the expression of TGFβig-h3 in tumor cells, and present finding of changes in stromal cell production of TGFβig-h3 indicates a more complex role than supposed previously.

These data show that TGFβig-h3 alone had little or no effect on myofibroblast or cancer cell proliferation and migration, although there was some stimulation of apoptosis. However, TGFβig-h3 strongly inhibited IGF-II-stimulated migration and proliferation of both cell types; knockdown of TGFβig-h3 expression increased the stimulatory effect of myofibroblast CM on cell migration; and in a xenograft model of myofibroblast-stimulated tumor growth, TGFβig-h3 had an inhibitory effect. The latter experiments employed SCID mice which have deficiencies in T- and B-cell maturation, making it unlikely that an immune response to TGFβig-h3 was involved. Moreover, the response to TGFβig-h3 is distinct from that to other proteins used in the same model (25). Previous work has established that gastric myofibroblasts produce IGF-II that can act as both an autocrine growth factor and a

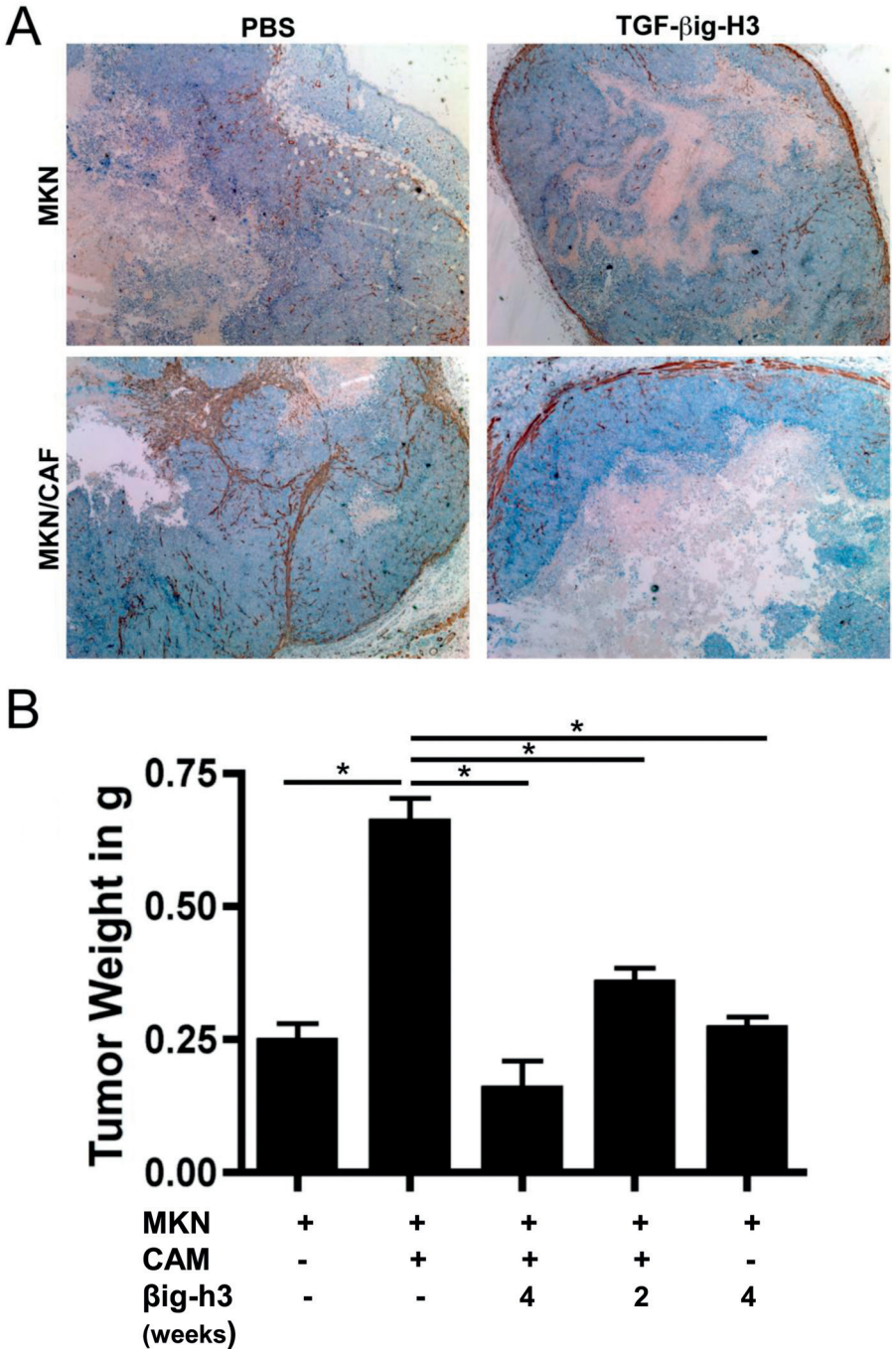

Fig. 6. Inhibitory effects of TGFβig-h3 in a xenograft model of stromal-stimulated tumor growth. (**A**) Representative images of α-SMA localization in xenografts and (**B**) quantification and statistical analysis of tumor volume. Mice were treated with TGFβig-h3 (1 μg per mouse per day) either for the whole duration of the experiment (4 weeks) or after 2 weeks of tumor growth. Treated xenografts were compared with untreated xenografts with and without co-injection of CAMs with MKN45 cells as appropriate. $n = 5$ per group, $^*P < 0.05$ and Dunnett for multiple comparisons; all data are represented as mean ± standard error of the mean.

paracrine stimulant of gastric epithelial cell proliferation and migration (23). The present findings extend this by showing that there are functional differences between CAMs and ATMs, and between CAMs based on tumor stage, in response to IGF-II. Moreover, inhibition of these effects by exogenous and endogenously generated TGFβig-h3 indicates that there is a dynamic equilibrium between stimulatory effects of IGF-II and inhibitory effects of TGFβig-h3 generated by stromal cells, that is lost in cancer progression. Interactions between TGFβig-h3 and IGF-II appear to occur proximal to activation of p42/44 MAPkinase which mediates the effects of IGF-II. There are RGB and FAS1 domains in TGFβig-h3 that mediate integrin binding; since there are well-recognized interactions between ECM proteins, integrins and IGF-receptor signaling (48), we suggest that the inhibitory action of TGFβig-h3 is exerted at this level.

Taken together, these data show myofibroblasts from gastric cancer differ from those from adjacent tissue in stimulating cancer cell proliferation, migration and invasion. By focusing on CAM secretomes, we have identified an unexpected role for myofibroblasts in restraining tumor migration and proliferation in early disease through secretion of TGFβig-h3. Depression of TGFβig-h3 secretion by myofibroblasts occurs with tumor progression and could provide a novel functional biomarker for stromal cell properties in cancer. Since TGFβig-h3 had

a suppressive effect in a xenograft model of stroma-stimulated cancer growth, we suggest that it may also be possible to develop novel therapeutic strategies based on the observation that stromal cell-stimulated tumor growth *in vivo* is prevented by restoration of TGFβig-h3.

Supplementary material

Supplementary methods and Supplementary Tables 1–5 and Figures 1–7 can be found at http://carcin.oxfordjournals.org/.

Funding

National Institute of Health (TMEM, 5 U54 CA126513-04/1); North West Cancer Research Fund (CR793); Deutsche Krebshilfe to M.Q.

Acknowledgements

We thank Dr Victoria Elliot for help with HPLC and acknowledge the technical assistance of Charlotte Woodcock with BrdU labeling and Fuksz Zoltanne with myofibroblast cultures.

Conflict of Interest Statement: None declared.

References

1. Bissell,M.J. *et al.* (2001) Putting tumours in context. *Nat. Rev. Cancer*, **1**, 46–54.
2. Tlsty,T.D. *et al.* (2006) Tumor stroma and regulation of cancer development. *Annu. Rev. Pathol.*, **1**, 119–150.
3. Saadi,A. *et al.* (2010) Stromal genes discriminate preinvasive from invasive disease, predict outcome, and highlight inflammatory pathways in digestive cancers. *Proc. Natl. Acad. Sci. U.S.A.*, **107**, 2177–2182.
4. Tuxhorn,J.A. *et al.* (2002) Reactive stroma in human prostate cancer: induction of myofibroblast phenotype and extracellular matrix remodeling. *Clin. Cancer Res.*, **8**, 2912–2923.
5. Kalluri,R. *et al.* (2006) Fibroblasts in cancer. *Nat. Rev. Cancer*, **6**, 392–401.
6. Bhowmick,N.A. *et al.* (2004) Stromal fibroblasts in cancer initiation and progression. *Nature*, **432**, 332–337.
7. Allinen,M. *et al.* (2004) Molecular characterization of the tumor microenvironment in breast cancer. *Cancer Cell*, **6**, 17–32.
8. Finak,G. *et al.* (2008) Stromal gene expression predicts clinical outcome in breast cancer. *Nat. Med.*, **14**, 518–527.
9. Farmer,P. *et al.* (2009) A stroma-related gene signature predicts resistance to neoadjuvant chemotherapy in breast cancer. *Nat. Med.*, **15**, 68–74.
10. Hagglof,C. *et al.* (2010) Stromal PDGFRbeta expression in prostate tumors and non-malignant prostate tissue predicts prostate cancer survival. *PLoS One*, **5**, e10747.
11. Coussens,L.M. *et al.* (2002) Inflammation and cancer. *Nature*, **420**, 860–867.
12. Erez,N. *et al.* (2010) Cancer-associated fibroblasts are activated in incipient neoplasia to orchestrate tumor-promoting inflammation in an NF-kappaB-dependent manner. *Cancer Cell*, **17**, 135–147.
13. Crawford,Y. *et al.* (2009) PDGF-C mediates the angiogenic and tumorigenic properties of fibroblasts associated with tumors refractory to anti-VEGF treatment. *Cancer Cell*, **15**, 21–34.
14. Orimo,A. *et al.* (2005) Stromal fibroblasts present in invasive human breast carcinomas promote tumor growth and angiogenesis through elevated SDF-1/CXCL12 secretion. *Cell*, **121**, 335–348.
15. Powell,D.W. *et al.* (2005) Epithelial cells and their neighbors I. Role of intestinal myofibroblasts in development, repair, and cancer. *Am. J. Physiol. Gastrointest. Liver Physiol.*, **289**, G2–G7.
16. Jiang,L. *et al.* (2008) Global hypomethylation of genomic DNA in cancer-associated myofibroblasts. *Cancer Res.*, **68**, 9900–9908.
17. Peek,R.M., Jr. *et al.* (2002) Helicobacter pylori and gastrointestinal tract adenocarcinomas. *Nat. Rev. Cancer*, **2**, 28–37.
18. Kamangar,F. *et al.* (2006) Patterns of cancer incidence, mortality, and prevalence across five continents: defining priorities to reduce cancer disparities in different geographic regions of the world. *J. Clin. Oncol.*, **24**, 2137–2150.
19. Correa,P. *et al.* (1994) Gastric cancer. *Cancer Surv.*, **19–20**, 55–76.
20. Weis,V.G. *et al.* (2009) Current understanding of SPEM and its standing in the preneoplastic process. *Gastric Cancer*, **12**, 189–197.
21. Wroblewski,L.E. *et al.* (2003) Stimulation of MMP-7 (matrilysin) by Helicobacter pylori in human gastric epithelial cells: role in epithelial cell migration. *J. Cell Sci.*, **116**, 3017–3026.
22. Hemers,E. *et al.* (2005) Insulin-like growth factor binding protein-5 is a target of matrix metalloproteinase-7: implications for epithelial-mesenchymal signaling. *Cancer Res.*, **65**, 7363–7369.
23. McCaig,C. *et al.* (2006) The role of matrix metalloproteinase-7 in redefining the gastric microenvironment in response to Helicobacter pylori. *Gastroenterology*, **130**, 1754–1763.
24. Houghton,J. *et al.* (2004) Gastric cancer originating from bone marrow-derived cells. *Science*, **306**, 1568–1571.
25. Quante,M. *et al.* (2011) Bone marrow-derived myofibroblasts contribute to the mesenchymal stem cell niche and promote tumor growth. *Cancer Cell*, **19**, 257–272.
26. Skonier,J. *et al.* (1992) cDNA cloning and sequence analysis of beta ig-h3, a novel gene induced in a human adenocarcinoma cell line after treatment with transforming growth factor-beta. *DNA Cell Biol.*, **11**, 511–522.
27. Billings,P.C. *et al.* (2002) The transforming growth factor-beta-inducible matrix protein (beta)ig-h3 interacts with fibronectin. *J. Biol. Chem.*, **277**, 28003–28009.
28. Skonier,J. *et al.* (1994) beta ig-h3: a transforming growth factor-beta-responsive gene encoding a secreted protein that inhibits cell attachment in vitro and suppresses the growth of CHO cells in nude mice. *DNA Cell Biol.*, **13**, 571–584.
29. Zhang,Y. *et al.* (2009) TGFBI deficiency predisposes mice to spontaneous tumor development. *Cancer Res.*, **69**, 37–44.
30. Ahmed,A.A. *et al.* (2007) The extracellular matrix protein TGFBI induces microtubule stabilization and sensitizes ovarian cancers to paclitaxel. *Cancer Cell*, **12**, 514–527.
31. Tang,J. *et al.* (2007) BetaIg-h3 is involved in the HAb18G/CD147-mediated metastasis process in human hepatoma cells. *Exp. Biol. Med. (Maywood)*, **232**, 344–352.
32. Ma,C. *et al.* (2008) Extracellular matrix protein betaig-h3/TGFBI promotes metastasis of colon cancer by enhancing cell extravasation. *Genes Dev.*, **22**, 308–321.
33. Sobin,L.H. *et al.* (2009) *TNM Classification of Malignant Tumours*. Wiley-Blackwell, Chichester.
34. Varro,A. *et al.* (2002) Gastrin-cholecystokinin(B) receptor expression in AGS cells is associated with direct inhibition and indirect stimulation of cell proliferation via paracrine activation of the epidermal growth factor receptor. *Gut*, **50**, 827–833.
35. Varro,A. *et al.* (2004) Helicobacter pylori induces plasminogen activator inhibitor 2 in gastric epithelial cells through nuclear factor-kappaB and RhoA: implications for invasion and apoptosis. *Cancer Res.*, **64**, 1695–702.
36. Pho,M. *et al.* (2008) Cofilin is a marker of myofibroblast differentiation in cells from porcine aortic cardiac valves. *Am. J. Physiol. Heart Circ. Physiol.*, **294**, H1767–H1778.
37. Kraman,M. *et al.* (2010) Suppression of antitumor immunity by stromal cells expressing fibroblast activation protein-alpha. *Science*, **330**, 827–830.
38. Desmouliere,A. *et al.* (2004) The stroma reaction myofibroblast: a key player in the control of tumor cell behavior. *Int. J. Dev. Biol.*, **48**, 509–517.
39. Bissell,M.J. *et al.* (2011) Why don't we get more cancer? A proposed role of the microenvironment in restraining cancer progression. *Nat. Med.*, **17**, 320–329.
40. Xu,B.J. *et al.* (2010) Quantitative analysis of the secretome of TGF-beta signaling-deficient mammary fibroblasts. *Proteomics*, **10**, 2458–2470.
41. Kannabiran,C. *et al.* (2006) TGFBI gene mutations in corneal dystrophies. *Hum. Mutat.*, **27**, 615–625.
42. Thapa,N. *et al.* (2007) TGFBIp/betaig-h3 protein: a versatile matrix molecule induced by TGF-beta. *Int. J. Biochem. Cell Biol.*, **39**, 2183–2194.
43. Irigoyen,M. *et al.* (2010) TGFBI expression is associated with a better response to chemotherapy in NSCLC. *Mol. Cancer*, **9**, 130.
44. Becker,J. *et al.* (2006) Keratoepithelin suppresses the progression of experimental human neuroblastomas. *Cancer Res.*, **66**, 5314–5321.
45. Wen,G. *et al.* (2011) TGFBI expression reduces in vitro and in vivo metastatic potential of lung and breast tumor cells. *Cancer Lett.*, **308**, 23–32.
46. Zhao,Y. *et al.* (2006) Loss of Betaig-h3 protein is frequent in primary lung carcinoma and related to tumorigenic phenotype in lung cancer cells. *Mol. Carcinog.*, **45**, 84–92.
47. Ween,M.P. *et al.* (2011) Transforming growth factor-beta-induced protein secreted by peritoneal cells increases the metastatic potential of ovarian cancer cells. *Int. J. Cancer*, **128**, 1570–1584.
48. Beattie,J. *et al.* (2010) Cross-talk between the insulin-like growth factor (IGF) axis and membrane integrins to regulate cell physiology. *J. Cell Physiol.*, **224**, 605–611.

Received March 8, 2012; revised April 26, 2012; accepted May 2, 2012